Proceedings of the 2006 WSEAS/IASME International Conference on Fluid Mechanics, Miami, Florida, USA, January 18-20, 2006 (pp1-6)

A Comparative Investigation into Aerodynamic Performances of Two Set Finned Bodies with Circular and Non Circular Cross Sections

MAHMOUD MANI and SHADI MAHJOOB
Aerospace Engineering Department
Amirkabir University of Technology
Hafez St., Enghelab St., Tehran, IRAN

Abstract: According to the advantages of noncircular bodies in storage and carriage purposes, these bodies have gained substantial attention by many researchers. In this paper, two circular and square (with rounded corners) bodies, which are attached to two fins, are studied in the free stream Mach number of 0.83. The cross section areas of bodies are the same. This work is done using experiment and CFD methods. In the CFD work, a three-dimensional, compressible, stationary, viscous, turbulent flow is simulated using FLUENT code with the standard k-ε model and adaptive grids. The comparison of the results of experiment and CFD simulation shows that the results of CFD are enough accurate. The experiment data in different angles of attack indicate that the square fin-body configuration has higher aerodynamic lift and drag coefficients than the circular one. Also, the results indicate the same aerodynamic performance for both bodies. The results of CFD confirm the deduction obtained from experiment and also they explain the aerodynamic parameters of different parts of fin-body configurations (body alones, bases of bodies, and fins) which are very considerable. The physics of flow is also studied using the pressure contours and velocity vectors.

Key-Words: Aerodynamics, Circular and Non-Circular Body Cross Sections, Experiment, Computational Fluid Dynamics

Nomenclature

CD	Drag Coefficient
CL	Lift Coefficient
L/D	Aerodynamic Performance

1 Introduction

In order to gain optimum aerodynamic performance and also to improve the bodies for transportation purposes, researcher's attentions have been towards the bodies with non-circular cross sections. Jackson and Sawyer [1] have experimentally investigated bodies with elliptical cross-sections and noticed a considerable increase in aerodynamic efficiency (L/D) for horizontal elliptical cross-sections (compared with circular cross-sections). Also, the work of Graves [2], which was performed for a wide range of Mach numbers (from subsonic to supersonic) around elliptic and circular cross-sectional bodies showed similar results. In family of bodies with non-circular cross-sections, because of the storage and carriage purposes, the ones with square or rectangular cross-sections (with round corners) are used more extensively. In 1987, Sigal and Lapidot [3] performed an extensive experimental investigation, in which three families of bodies with same length and cross-sectional areas were used. Their results showed that C_N was the highest for the horizontal rectangular case and the second highest for the square case. Of course, the problem with the rectangular case is that, when the body rolls and its cross-section changes from horizontal rectangle to vertical one, its aerodynamic efficiency drops drastically (even to less than the circular case). Note, their results were consistent in both cases of a body with and without fins.

Mahjoob and Mani [4] studied the circular and square body alones in a transonic flow using experiment, CFD, and semi-empirical methods. The results of their work indicate that a change of the cross section from circular to square leads to the increase of the aerodynamic parameters (lift coefficient, drag coefficient, and aerodynamic performance). In addition, at low angles of attack, the change of the cross section (from circular to square) not only increases the lift coefficient and aerodynamic performance very considerably, but also does not affect drag coefficient very much. In fact, changing the cross section from circular to square in order to increase the aerodynamic performance is more successful and effective at low angles of attack.

Flow separation effects are highly related to the corners of the square or rectangular cross-sections and cause unfavorable aerodynamic instabilities [5]. Mahjoob and Mani [6] studied the effects of fin-body interference in square and circular bodies experimentally. The results indicate that the fin-body interference of circular body is higher than that of the square one.

2 Models and Characteristics

Two different bodies, one having circular cross section and the other having square cross section with rounded corners, are simulated in body-fin configuration (Fig. 1). Both bodies have the same body length and cross section area. The bodies have fineness-ration-3.5 ogive noses and cylindrical after bodies, giving overall fineness ratio of 10.5. The wings have 47° sweepback angles, aspect ratios of 3.5, taper ratios of 0.2, and hexagonal sections of 6% thickness, as showing in Fig.1. The fin span (the distance between the tips of the fins) in both models of circular and square is the same and the aerodynamic parameters in this study is calculated based on the cross section area which is equal to 0.001257 m^2. The free stream Mach number is 0.83, the static temperature is 266.86K, the static pressure is 54400Pa, and the total pressure is 85000Pa.

3 Experimental Facilities

The experimental test has been done in a multi purposed ST-2 wind tunnel. The tunnel is designed and calibrated for subsonic, transonic, and supersonic regimes for Mach numbers of 0.4 to 2.2. The test section is 60Cm × 60Cm. Its nozzle is flat and controllable and the nozzle's geometry can be changed during the test. This is done by seven double handle and electrical jacks. Tunnel's power is produced by a turbofan engine with the power of 100000KW whose control is done by remote control electro mechanically. The range of angle of attack is from -2° to 16°. The accuracy of models' manufacturing is about 0.01 mm.

4 Computational Methodology

The FLUENT CFD code [7], which uses a cell centered finite volume method and has been proven to work well for different flow regimes around bodies, is used in this study. The explicit method implemented uses a coupled solution method. Note, all the schemes used here are second order. The SIMPLE algorithm with under-relaxation coefficients is used in the overall discretization of the equations. In order to reduce the dispersion errors (and also to increase the speed of the computations), the multi-grid approach is also used.

Because of the complexity of geometry of models, existence of transonic flow, and also solving full Navier Stocks equations, with considering viscosity and turbulence, it took more than 10,000 iterations for convergence. So that the residuals are lower than 1×10^{-4}. Also, each of iterations took a lot of time. In order to increase the accuracy of the results, adaptive grids were used.

4.1 Governing Equations and Physical Properties

The Reynolds averaged governing equations include continuity, momentum, and energy which are as follows:

$$\frac{\partial}{\partial x_i}(\rho u_i) = 0$$

$$\frac{\partial}{\partial x_i}(\rho u_i u_j) = -\frac{\partial p}{\partial x_i} + \frac{\partial \tau_{ij}}{\partial x_j} + \rho g_i + F_i$$

$$\frac{\partial}{\partial x_i}(\rho u_i h) = \frac{\partial}{\partial x_i}\left[K\frac{\partial T}{\partial x_i}\right] + u_i\frac{\partial p}{\partial x_i} + \tau_{ij}\frac{\partial u_i}{\partial x_j},$$

where

$$\tau_{ij} = \left[\mu_{eff}\left(\frac{\partial u_i}{\partial x_j} + \frac{\partial u_j}{\partial x_i}\right)\right] - \frac{2}{3}\mu_{eff}\frac{\partial u_l}{\partial x_l}\delta_{ij};\ \mu_{eff} = \mu + \mu_T.$$

The flow considered here is three-dimensional, compressible, stationary, single-phase, viscous and turbulent that the standard κ-ε model is used for turbulence modeling. The fluid is air, for which the viscosity is obtained using Sutherland relation and density is obtained using ideal gas relation. The turbulence intensity is 1%, the characteristic length scale (the body's diameter of cross-section) is 0.04m.

4.1.1 Turbulence Modeling

The standard $k-\varepsilon$ model with the standard wall functions [8] is used in this study. Recall that, in $k-\varepsilon$ model, the averaged Reynolds stresses are taken proportional to the averaged velocity gradients and the proportionality constant (μ_T) is found from k and ε equations. The turbulent kinetic energy, k, and its rate of dissipation, ε, are obtained from the following transport equations:

$$\rho\frac{Dk}{Dt} = \frac{\partial}{\partial x_i}\left[\left(\mu + \frac{\mu_t}{\sigma_k}\right)\frac{\partial k}{\partial x_i}\right] + G_k - \rho\varepsilon - Y_M,$$

and

$$\rho\frac{D\varepsilon}{Dt} = \frac{\partial}{\partial x_i}\left[\left(\mu + \frac{\mu_t}{\sigma_\varepsilon}\right)\frac{\partial \varepsilon}{\partial x_i}\right] + C_{1\varepsilon}\frac{\varepsilon}{k}(G_k) - C_{2\varepsilon}\rho\frac{\varepsilon^2}{k}$$

In addition, the standard wall functions, based on the work of Launder and Spalding were used [9].

4.2 Geometric Modeling

In Fig. 1, the bodies' geometry and cross sections are presented. The computational domain around bodies, is assumed to be a cylinder whose diameter is 21 times half of the span of the bodies (Fig.2). The other outer boundaries are assumed to be 5 body lengths at the front and 5 body lengths behind the bodies (Fig. 2). This size of the domain is shown to be optimal using numerical experimentation. Note, due to the symmetric assumption used, only half of the domain is considered here. Our computational results indicate that this assumption does not affect the results considerably.

4.3 Computational Grid

A blocked structured, body fitted, and non-uniform grid is used in this study (Figs. 3 and 4). The grid was clustered around the bodies and fins and also in sensitive region (with high pressure and velocity gradients). Because of the complexity of body geometries and the existence of sweepback fins, 31 blocked were created. After grid resolution study, a 364,000 cells grid is chosen as the basic grid (Figs. 3 and 4). To insure grid insensitivity, adaptions are made on Y^+ and pressure gradients.

4.4 Boundary Conditions

Different boundaries of the physical domain are used in this work (Fig.2). The wall of the body and fins are assumed to be adiabatic (A). The free stream pressure is assumed at the inlet (B) and outlet (C) of the domain. In the pressure outlet boundary condition, only the static pressure is specified and all other flow quantities are extrapolated from the flow in the interior. The far field pressure condition is also used (D).This boundary condition is often called a characteristic boundary condition because it uses characteristic information (Reiman invariants) to determine the flow variables at the boundaries. At the symmetric plane, the symmetric boundary condition is implemented (E) and the axis boundary is used at two axis of front and behind body (F).

5 Results

In this work, the aerodynamic parameters of square and circular fin-body cross sections have been compared

using experimental and computational methods. The results are presented as follows.

5.1 Experimental Results:

Fig. 5 which shows the lift coefficient of bodies indicates that changing the cross section from circular to square increases the lift coefficient. Figure 6 shows the drag coefficient of bodies. This figure indicates that at all angles of attack, the body with square cross section has more drag coefficient than the circular one. Since the increase percentage of lift and drag coefficients are somehow the same, the aerodynamic performance (L/D) of circular and square bodies are very similar (Fig.7).

5.2 Computational Results

In order to study the effects of cross section on the aerodynamic parameters of different parts of fin-bodies (such as body alones and fins separately) and also to study the physics of flow which could not be achieved by experimental data, two circular and square fin bodies are simulated using computational methods. In addition to study the effects of changing the angle of attack on the physics of flow, the circular body is also simulated at 16.27° angle of attack.

At first, to validate the computational results, the experimental and computational results are compared and then the aerodynamic parameters of bodies and the physics of flow (using total pressure contours and velocity vectors at different situations) are studied.

5.2.1 Code Validation Study

Comparison of experimental and computational data shows a good agreement and accuracy. In CFD results, at zero angle of attack, the lift coefficient of bodies are zero which is completely true because the bodies are symmetric. As it is shown at table 1, the drag coefficient obtained from experiment and CFD are very close to each other and the difference at zero angle of attack is under 12%. The error of lift and drag coefficients obtained from CFD for circular body at 16.27° angle of attack is under 5%.

One of the main reasons of errors especially at low angles of attack is related to the base drag. In fact, in experimental test, the bases of the bodies are attached to the after body so its setup is different from CFD simulation where flow can move behind the bodies and create the wake and so increase the base drag. Although, the drag obtained from the base surface of the bodies are reduced from the CFD results for validation study, there are still some effects of flow physics behind the body on the area around the bodies which can affect the aerodynamic parameters. It is also noticeable that because of lack of drier system or filter in the wind tunnel, the results can have a little error. It happens especially at high speed (supersonic regimes) that the air flow reaches the two phase flow situation.

5.2.2 Effects of Cross Section on Aerodynamic Parameters

In this work, the pressure and friction drags caused by different parts of the circular and square fin-body configurations are studied. In the circular body at zero angle of attack, about 54.68% of drag is belonged to the pressure drag and 45.32% of drag is belonged to the friction drag. 29.1% of the drag is caused by the fins in which 10% of the drag is belonged to the pressure drag of fins and 19.1% of the drag is belonged to the friction drag of fins. In addition, 33.1% of drag is belonged to the base drag. The rest, 37.8% of drag is caused by the body alone (without considering fins and bases). In fact, 11.56% of the drag is belonged to the pressure drag and 26.24% of the drag is belonged to the friction drag.

In the square body at zero angle of attack, about 52.6% of drag is belonged to the pressure drag and 47.4% of drag is belonged to the friction drag. 30.3% of the drag is caused by the fins in which 9.8% of the drag is belonged to the pressure drag of fins and 20.5% of the drag is belonged to the friction drag of fins. In addition, 32.4% of drag is belonged to the base drag. The rest, 37.3% of drag is caused by the body alone (without considering fins and bases). In fact, 10.4% of the drag is belonged to the pressure drag and 26.9% of the drag is belonged to the friction drag.

The above percentages show that the drag distribution is very similar in both circular and square bodies. However, there are some interesting differences between these two bodies. At zero angle of attack, the drag coefficient of square fin-body is a bit higher than that of the circular fin-body. The comparison of the drag coefficients of circular and square body alones (without considering the bases) indicates that the pressure drag of square body alone is lower than that of the circular body alone. While, the friction drag of square body alone is higher than that of the circular one. This is because, although the areas of circular and square cross sections are equal, the perimeter of square cross section is more than that of the circular one so the area of the square body alone is more than that of the circular body alone. Totally, the drags of both body alones are somehow the same.

Since the span of fins (distance between the tips of fins) is the base for circular and square body-fin configurations, and regarding to smaller width of square cross section than that of circular one, the fins attached to the square body are larger than those of the circular body so the friction drag of fins attached to the square body is higher than that of the circular body which results in a bit higher drag coefficient for square fin-body configuration. At zero angle of attack, because of the symmetry of fin-bodies, the lift coefficients of both fin-bodies is equal to zero.

5.2.3 Physics of Flow

Figures 8 and 9 indicate the total pressure contour at circular and square fin-body configurations at zero angle of attack. At both figures, the stagnation region is located around the nose of the bodies. Also, the least pressure is located at the bases of the bodies. The study of maximum and minimum pressure show that the maximum pressure of the circular body is higher than

that of the square body and the minimum pressure of the circular body is lower than that of the square body. Therefore, the pressure difference between the front and behind the bodies, which makes the pressure drag, in circular fin-body configuration is higher than that of the square one. This deduction is also presented in Table 2. The study of Figs. 8 and 9 also shows a high pressure at the leading edge of fins. The effects of fin-body interactions are also seen at these figures which are accompanied with the decrease of the total pressure.

In Fig. 10, the total pressure contour at circular fin-body configurations at 16.27° angle of attack is presented. According to Figs 8 and 10, by increasing the angle of attack, the stagnation region is moved to under the body and a pressure difference is created between the above and below the body which resulted in lift force. The study of total pressure contour over and below the fins is also noticeable. Increasing the angle of attack (Fig.10) decreases the pressure over the fins considerably, especially near the leading edge, which results in a high pressure difference between over and below the fins and so a considerable lift force. Comparing Figs 8 and 10 which shows the effects of changing the angle of attack indicates that at zero angle of attack, total pressure contours over and below the body are similar and symmetry that results in zero lift coefficient. However, at 16.27° angle of attack, the distribution of pressure contours over and below the body is very different. In addition, study of the maximum and minimum pressure of circular fin-body configuration (Figs. 8 and 10) indicates that by increasing the angle of attack, the pressure difference increase very considerably which results in higher pressure drag. It is noticeable that at 16.27° angle of attack (Fig.10), the minimum pressure over the leading edge of the fins is even less than that of the wake region 9behind the body).

In Figs. 11 and 12, velocity vectors at the bases of the circular and square bodies and the symmetry plane are presented at zero angle of attack. Behind the bodies, there are two symmetry wakes whose centers are located at a quarter of cross sections' width from the center of cross sections. In these figures, the symmetry of wakes on the bases of bodies and the symmetry plane of domain are presented. The length of the vectors shows the velocity magnitudes, which are very small in the wake region, and shows the small or zero velocity magnitudes. Figs. 11 and 13 indicate that increasing the angle of attack, damages the symmetry of flow streamlines and wakes. In addition, increasing the angle of attack (Fig. 13) decreases the wake region area which is destroyed by the main-flow more rapidly than the smaller angles of attack.

References:

[1] Jackson, C.M. and Sawyer, W.C., "Bodies with Non-Circular Cross-Sections and Bank-to-Turn Missiles," Progress in Astronautics and Aeronautics, Vol. 141, pp. 365-389, 1991.

[2] Graves, E.B., "Aerodynamic Characteristics of a Mono-Planar Missile Concept with Bodies of Circular and Elliptical Cross-Sections," NASA TM-74079, Dec. 1977.

[3] Sigal, A. and Lapidot, E., "The Aerodynamic Characteristics of Configurations Having Bodies with Square, Rectangular, and Circular Cross-Sections at a Mach Number of 0.75," AIAA, Inc., 1987.

[4] Mahjoob, S. and Mani, M., "The Ability of CFD Methods to Study Noncircular Bodies", Presented and Published in the Proceedings of ICCMSE 2004, International Conference of Computational Methods in Sciences and Engineering, Greece, November 2004.

[5] Nielsen, J.N., "Problems Associated with the Aerodynamic Design of Missile Shapes," Proceedings of the Second Symposium on Numerical and Physical Aspects of Aerodynamic Flows, CA, Jan. 1983.

[6] Mahjoob, S., Mani, M., Ebnoldin, H., Haghiri, A., "Aerodynamic Study of Bodies with Non-Circular Cross Section Using Experimental Method", Published in the Proceedings of The 8th Inter. Conf. of Iranian Society of Mechanical Engineers, Tehran, Iran, May 2004.

[7] "FLUENT 5 User's Guide," FLUENT Incorporated, 1998.

[8] Launder, B.E. and Spalding, D.B. "Lectures in Mathematical Models of Turbulence", Academic Press, London, England, 1972.

[9] Launder, B. E., and Spalding, D. B., "The Numerical Computation of Turbulent Flows," *Journal of Computer Methods in Applied Mechanics and Engineering*, Vol. 3, 1974, pp. 269-289.

Table 1: Drag Coefficients of circular and square fin-body configurations.

Drag Coefficient	Circular, 0° angle of attack	Square, 0° angle of attack	Circular, 16.27° angle of attack
Experiment	0.2521	0.252	3.2018
CFD (without bodies' base drag)	0.277	0.282	3.36

Table 2: Drag Coefficients of different parts of the bodies at zero angle of attack.

	CD	CD_{pr} (Pressure)	CD_F (Friction)	CD_B (Base)	CD_{Fins}	$CD_{Fins,Pr}$ (Pressure)	$CD_{Fins,F}$ (Friction)	CD_{Body} (Body Alone Without Bases)	$CD_{Body,Pr}$ (Pressure)	$CD_{Body,F}$ (Friction)
Circular	0.414	0.226	0.188	0.137	0.12	0.041	0.079	0.156	0.048	0.109
Square	0.417	0.219	0.198	0.135	0.126	0.041	0.085	0.155	0.043	0.112

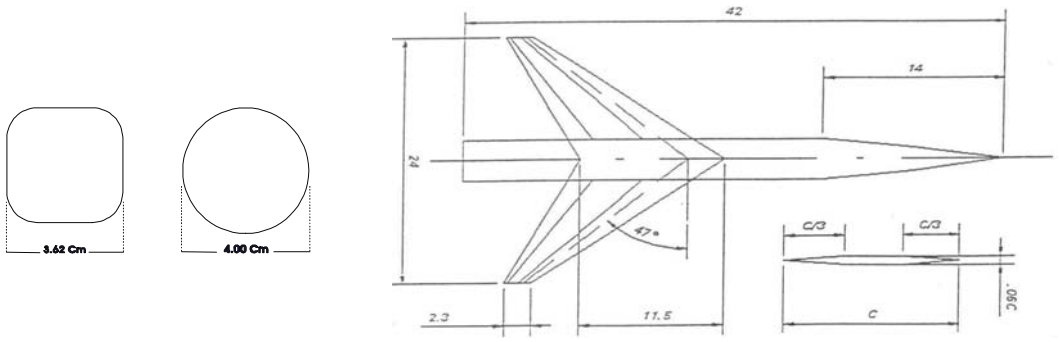

Fig1. The geometry of body and cross sections, circular and square with rounded corners.

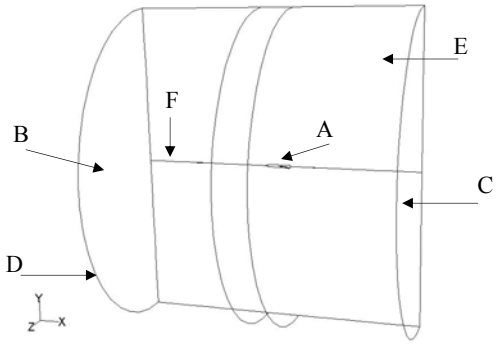

Fig. 2. The computational domain and boundary conditions.

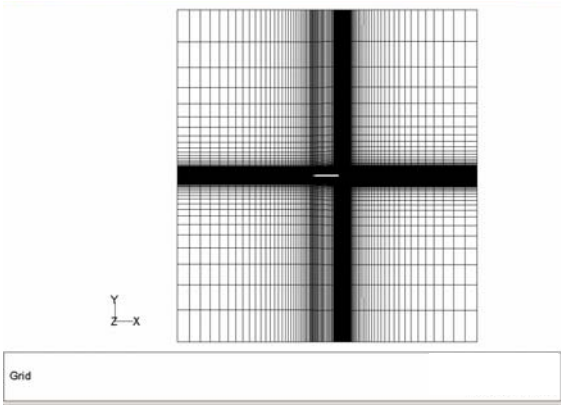

Fig. 3. The computational grid at the symmetry plane of the domain (before adaption).

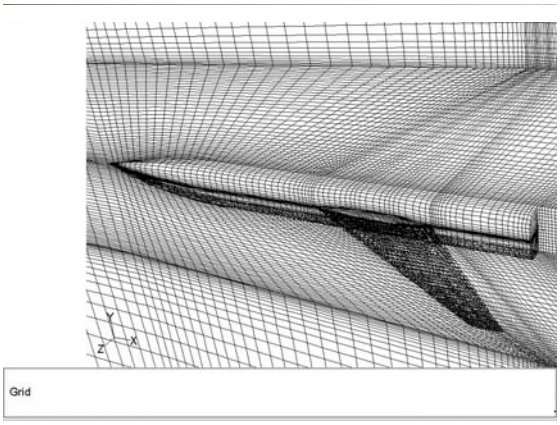

Fig. 4. The computational grid at the symmetry plane, the body and the fin (before adaption).

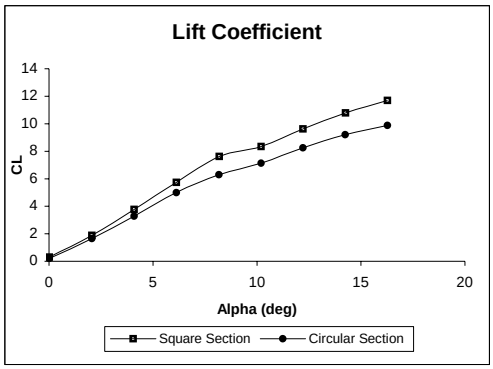

Fig.5. Lift coefficient of circular and square fin-bodies obtained from experimental test.

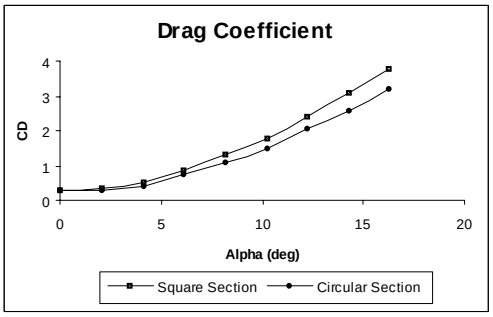

Fig.6. Drag coefficient of circular and square fin-bodies obtained from experimental test.

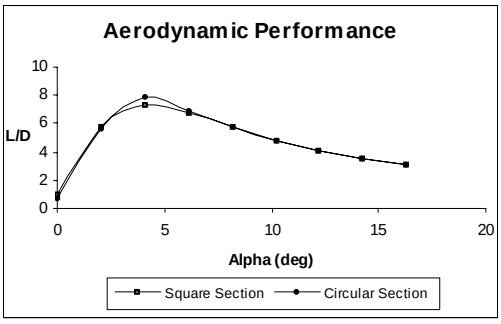

Fig.7. Aerodynamic performance of circular and square fin-bodies obtained from experimental test.

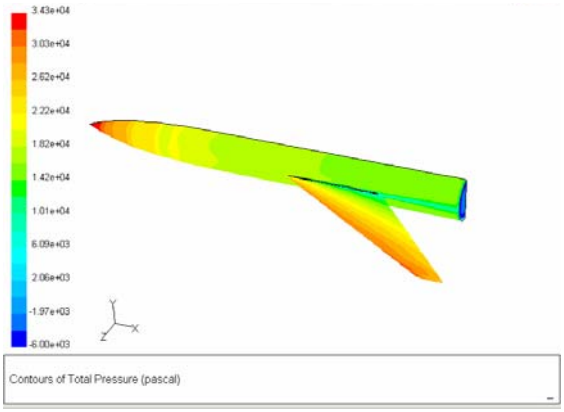

Fig.8. Total pressure contour at circular fin-body at 0° angle of attack.

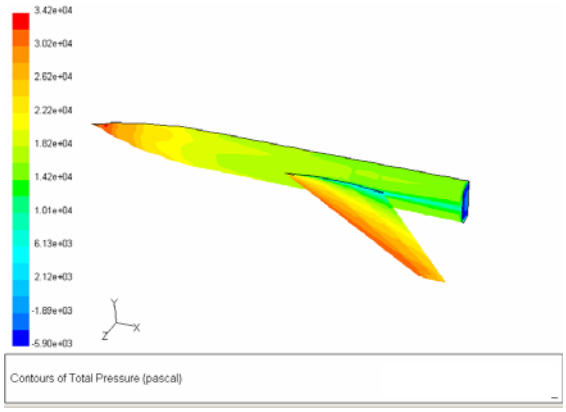

Fig.9. Total pressure contour at square fin-body at 0° angle of attack.

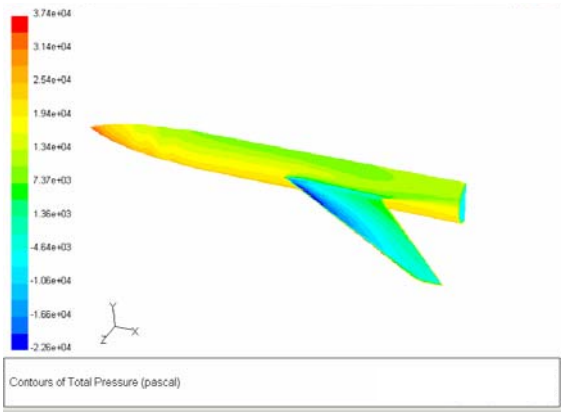

Fig.10. Total pressure contour at circular fin-body at 16.27° angle of attack.

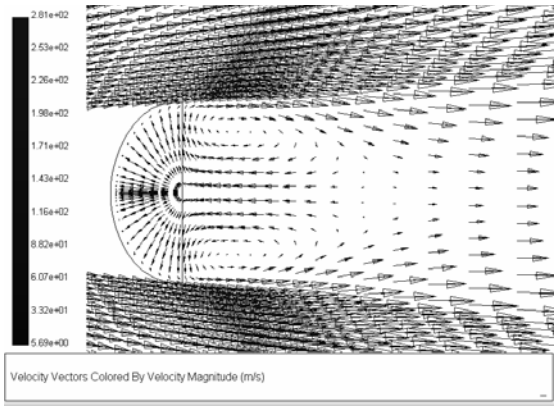

Fig. 11. Velocity vectors at the base of circular fin-body and the symmetry plane of the domain at 0° angle of attack.

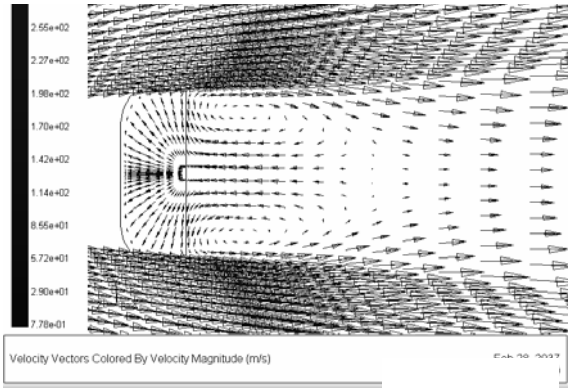

Fig. 12. Velocity vectors at the base of square fin-body and the symmetry plane of the domain at 0° angle of attack.

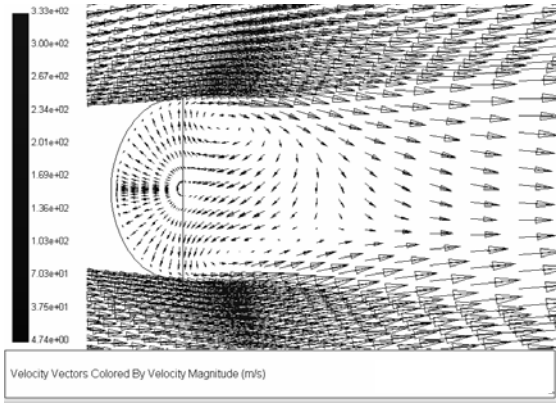

Fig. 13. Velocity vectors at the base of circular fin-body and the symmetry plane of the domain at 16.27° angle of attack.